INTERNATIONAL JOURNAL FOR NUMERICAL METHODS IN FLUIDS, VOL. 21, 683–696 (1995)

A COMPARISON STUDY ON MULTIVARIANT AND UNIVARIANT FINITE ELEMENTS FOR THREE-DIMENSIONAL INCOMPRESSIBLE VISCOUS FLOWS

TONY W. H. SHEU AND MORTEN M. T. WANG

Institute of Naval Architecture and Ocean Engineering, National Taiwan University, 73 Chou-Shan Rd., Taipei, Taiwan, Republic of China

SUMMARY

In this paper, four quadratic hexahedron elements are considered and assessed for analysis of an incompressible viscous flow underlying the mixed finite element method. We classify the investigated elements as multivariant and univariant finite elements. With the same number of pressure unknowns, multivariant elements are more constrained when the number of elements per side is larger than 10, as compared with that of continuous pressure elements. In multivariant elements, the coding is complicated by the appearance of restricted degrees of freedom at mid-face and mid-edge nodes. The comparison consequently should be made via numerical example against the analytical problem.

KEY WORDS: multivariant; univariant

1. INTRODUCTION

The finite element method has now been used for more than three decades and has recently emerged as a reliable analysis tool for industrial applications. Historically, several formulations underlying the finite element theory have been developed for incompressible fluid flows, among which the mixed formulation has been most used and is still a rapidly evolving subject.[1–3] Other viable alternatives formulated on the basis of primitive variables comprise the penalty[4] and least-squares finite element methods.[5,6] These methods have advantages of being tied to the legitimate boundary conditions.[4–8] No artificial boundary condition needs to be devised in the intermediate steps as required in the segregated formulations.[9,10] While being a storage intensive approach, we believe the merits gained in the mixed formulation outweigh the drawbacks. In this paper, no attempt will be devoted to justifying this view point.

In finite element computations of incompressible flows, numerical difficulties are mainly associated with the discrete divergence-free condition and pressure instability.[11,12] In the past, erroneous results were obtained at times from many elements because they fell short of the inf-sup (or LBB) condition. These oscillatory pressure modes are the consequence of an inappropriate combination of interpolation functions for the velocities and pressure. Thanks to the work of Brezzi[13] and Babuška,[14] we now understand that as finite element practioners we should use different basis functions to interpolate velocity and pressure in the context of the mixed method. An examination of existing literature reveals that quite a few convergent pairs have been devised. As to three-dimensional incompressible flow simulations, it is particularly difficult to justify if an element is accommodated with the LBB (Ladyzhenskaya–Babuška–Brezzi) condition. To dispense with this constraint, recently, a least-squares

CCC 0271–2091/95/080683–14

Received September 1994
Revised March 1995

finite element model was successfully developed.[5,6,15] By means of minimization procedure, stable solutions are rendered regardless of the LBB condition.

The emphasis here is placed on seeking several appropriately arranged three-dimensional elements. Comparison studies were made among these elements by evaluating the computed solutions.

2. MATHEMATICAL MODEL

We consider an incompressible fluid at the laminar flow regime. As regards dependent variables, there exist several settings such as the velocity-pressure,[16] streamfunction-vorticity,[16] velocity-vorticity,[17] and vorticity-vector potential,[18] among which the velocity-pressure is an appealing choice since it pertains to legitimate boundary conditions.[4,7,8] No artificial boundary conditions need be imposed in the intermediate projection steps. In a domain Ω of three dimensions, the steady solution sought is from the following dimensionless governing equations:

$$(\underline{u} \cdot \nabla \underline{u}) = \frac{1}{Re} \nabla^2 \underline{u} - \nabla p, \tag{1}$$

$$\nabla \cdot \underline{u} = 0. \tag{2}$$

In equation (1), Reynolds number Re is defined by

$$Re = \rho u_{\text{ref}} L_{\text{ref}} / \mu. \tag{3}$$

To close the above elliptic system, we need to specify the following boundary conditions on Γ_D and Γ_N, respectively:

$$\underline{u} = \underline{f} \quad \text{on } \Gamma_D, \tag{4}$$

$$-p\underline{\mathbf{n}} + \frac{1}{Re} \frac{\partial \underline{u}}{\partial n} = \underline{g} \quad \text{on } \Gamma_N. \tag{5}$$

It is noteworthy that $\Gamma = \partial\Omega = \Gamma_D + \Gamma_N$. In equation (5), $\underline{\mathbf{n}}$ stands for the unit outward normal vector. For simplicity, we only consider boundary conditions of the Dirichlet type as shown in (4). In incompressible flow analyses, the divergence-free constraint condition placed on the velocity field should be carefully considered. This subject has truly dominated researches for more than 20 years. Another important issue concerns the pressure, which is nothing but the Lagrangian multiplier[1] rather than the thermodynamic property in the compressible counterpart where an equation of state is indispensable.

3. FINITE ELEMENT MODEL

Discretization of coupled equations (1) and (2) is most often accomplished by using a method of weighted residuals. Of central importance to a finite element program capable of yielding better discrete ellipticity under a high Reynolds number is finding an appropriate biased weighting so that more upwind information is considered. In integrating these conservation equations, we proceed in the same way as the Petrov–Galerkin method does. This leads to the weighted residuals statement: For admissive functions $\underline{w} \in H_0^1(\Omega) \times H_0^1(\Omega)$ and pressure mode $q \in L^2(\Omega)/\mathscr{R} = P$, find the velocity-pressure pair $(\underline{u}, p) \in V \equiv (H_0^1 \times H_0^1) \times P$ from

$$\int_\Omega (\underline{u} \cdot \nabla)\underline{u} \cdot \underline{w} \, d\Omega + \frac{1}{Re} \int_\Omega \nabla \underline{u} : \nabla \underline{w} \, d\Omega - \int_\Omega p \nabla \cdot \underline{w} \, d\Omega = 0 \quad \forall \underline{w} \in H, \tag{6}$$

$$\int_\Omega (\nabla \cdot \underline{u}) q \, d\Omega = 0 \quad \forall_g \in P, \tag{7}$$

subject to the essential boundary condition $\underline{u} = \underline{f}$ on $\partial\Omega$. Let $\underline{w}$ be test functions and $N(\underline{x})$ and $M(\underline{x})$ be trial functions so that $\underline{u}^h = \Sigma \underline{u}^i N_i$, $p^h = \Sigma p^i M_i$. We will discuss them in more detail in sections 3.1 and 3.2. Substituting these test and basis functions into the above constrained variational statement, the matrix equations take the following form where the biased weighting functions are only applied to the nonlinear terms:

$$\underline{\underline{A}}\,\underline{\lambda} = \underline{b} \tag{8}$$

where

$$\mathbf{A} = \int_{\bar{\Omega}^h} \begin{Bmatrix} C^{il} & 0 & 0 & -M^l \dfrac{\partial N^i}{\partial X_1} \\ 0 & C^{il} & 0 & -M^l \dfrac{\partial N^i}{\partial X_2} \\ 0 & 0 & C^{il} & -M^l \dfrac{\partial N^i}{\partial X_3} \\ M^i \dfrac{\partial N^l}{\partial x_1} & M^i \dfrac{\partial N^l}{\partial X_2} & M^i \dfrac{\partial N^l}{\partial X_3} & 0 \end{Bmatrix} \mathrm{d}\bar{\Omega}^h, \tag{9}$$

$$\lambda = \{V_1^l, V_2^l, V_3^l, P^l\}^{\mathrm{T}}, \tag{10}$$

$$C^{il} = (N^i + \bar{P}^i)(N^l \tilde{V}_j^l) \frac{\partial N^l}{\partial X_j} + \frac{1}{Re} \frac{\partial N^i}{\partial x_j} \frac{\partial N^l}{\partial X_j}, \tag{11}$$

$$\bar{P}^i = \tau (N^l \tilde{V}_j^l) \frac{\partial N^i}{\partial X_j}, \tag{12}$$

$$\underline{b} = -\int_{\Gamma^h_{\mathrm{out}}} N^i \begin{Bmatrix} pn_x - \dfrac{1}{Re} \dfrac{\partial u}{\partial n} \\ pn_y - \dfrac{1}{Re} \dfrac{\partial v}{\partial n} \\ pn_z - \dfrac{1}{Re} \dfrac{\partial w}{\partial n} \\ 0 \end{Bmatrix} \mathrm{d}\Gamma^h. \tag{13}$$

As is usual in the mixed formulation, the stiffness matrix is neither symmetric nor positive-definite. Moreover, improper interpolatory combinations of p and $\underline{u}$ may render this matrix singular. Such a circumstance might yield spurious zero eigenvalues and terminate the calculation. As a consequence, some precautions must be taken to cope with the so-called pressure modes.

3.1. Basis functions for primitive variables

Finite elements applicable to three dimensional simulations are usually categorized as tetrahedral and hexahedral elements. Whether one class of elements is favored over another depends on the target problem under consideration. We will only consider hexahedral elements for the time being. Of

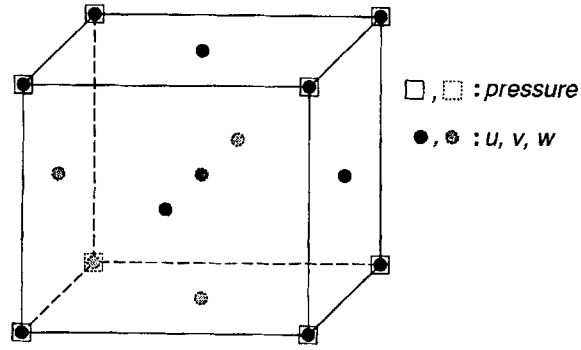

Figure 1. Primitive variables stored in a 15/8 element

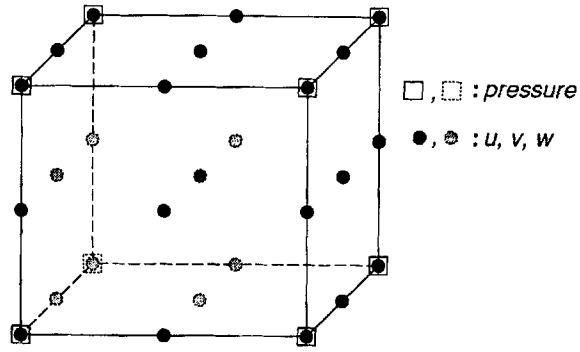

Figure 2. Primitive variables stored in a 27/8 element

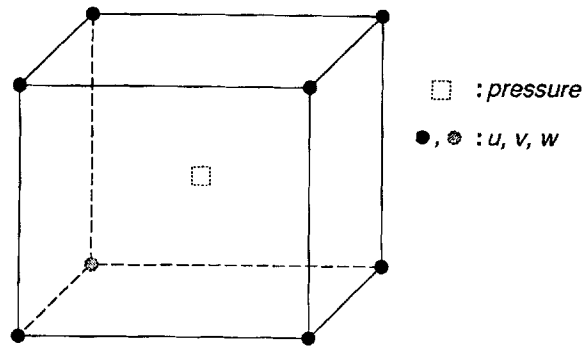

Figure 3. Primitive variables stored in a 8/1 element

importance in the above matrix equations is the selection of trial finite element spaces for p and $\underline{u}$. The matter of making an appropriate combination will be dealt with later.

For reasons of consistency, the polynomial order for the pressure unknowns must be one order lower than that for the velocities. Evidently, equal-order interpolations for the velocity and pressure tend to yield an erroneous pressure distribution unless the finite element analysis formulated is based on the idea of least squares. Two types of pressure approximations are possible, either continuous or discontinuous. In the continuous context, a trilinear interpolation is employed by lodging the pressure

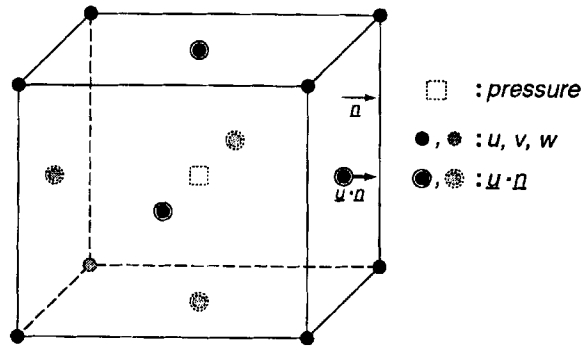

Figure 4. Primitive variables stored in a 14/1 element

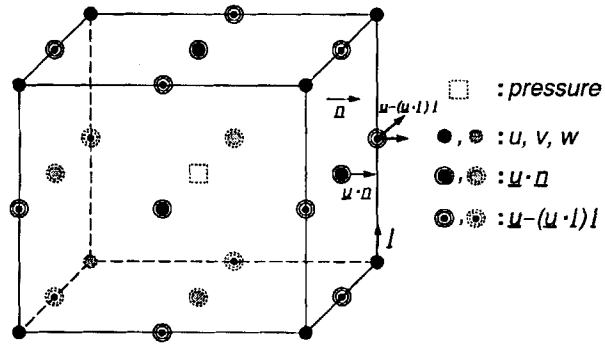

Figure 5. Primitive variables stored in a 26/1 element

degrees of freedom at eight vertices of the element. As for the discontinuous setting, the pressure node is logically placed on the element centroid. Given these means of storing pressure unknowns, velocity nodal points can be chosen accordingly. In the first setting, shown in Figures 1 and 2, the polynomials for approximating the pressure should be one order lower than those for the velocities. For completeness, we will also discuss the so-called Q_1P_0 element, shown in Figure 3. Elements falling into the second catalogue are called the multivariant finite elements, shown in Figures 4 and 5, following the terminology of Gupta *et al.*[19]

The finite element, shown in Figure 3, is believed to be the simplest conforming mixed element applicable to three-dimensional flow analyses. This element, defined by using the trilinear-velocity/constant-pressure basis functions, involves eight nodal points, which does not suffice in itself to produce stable pressures. Therefore, we will not take this element into consideration. Of note is that the undermined pressure solutions may coexist with a set of smooth and accurate velocity solutions. To surmount the difficulty regarding these oscillatory pressures, we can regularize this wavy system by modifying the continuity equation in a manner such that the stabilization condition is achieved.

3.1.1. Continuous pressure elements. In the context of continuous pressure elements, two elements are considered which assign pressure nodal points at eight vertexes of a hexahedron. Since the pressure serves as a Lagrangian multiplier when an incompressible flow is considered, an element of 24 degrees of freedom defined at eight nodal points fails to render smooth pressure solutions at the same number of vertex nodes (8 degree of freedom). This implies that the divergence-free condition is not strongly tied to this arrangement. This fact may explain why this element is generally afflicted with spurious

pressure modes. Given this, it is of necessity to reserve more velocity nodal points to enhance the discrete ellipticity. Among the possible higher-order velocity elements, we consider herein the following two alternatives.

3.1.1.1. Trilinear-pressure/15 velocity element (or 15/8 element). As mentioned earlier, numerical oscillations in a 8/8 element are caused by an approximation free of the inf-sup condition. As a remedy, we could add more nodes to the element shown in Figure 6. In the first place, we allocate one velocity node to each face and centroid of a hexahedron. The resulting element has 15 velocity nodal points or 45 degrees of freedom. We refer herein to this element as a 15/8 element which is defined by a tri-linear continuous pressure field and the following basis functions for velocities in a tri-quadratic element.[20]

Corner node:

$$N_i = \tfrac{1}{2}(1+\bar{\xi})(1+\bar{\eta})(1+\bar{\zeta})(\bar{\xi}\bar{\eta}+\bar{\eta}\bar{\zeta}+\bar{\zeta}\bar{\xi}-2\bar{\xi}\bar{\eta}\bar{\zeta}). \tag{14a}$$

Mid-face node:

$$N_i = \tfrac{1}{2}[\bar{\xi}(1+\bar{\xi})+\bar{\eta}(1+\bar{\eta})+\bar{\zeta}(1+\bar{\zeta})](1-\xi^2+\bar{\xi}^2)(1-\eta^2+\bar{\eta}^2(1-\zeta^2+\zeta^{-2}). \tag{14b}$$

Centre node:

$$N_i = (1-\xi^2+\bar{\xi}^2)(1-\eta^2+\bar{\eta}^2)(1-\zeta^2+\bar{\zeta}^2), \tag{14c}$$

where

$$\bar{\xi} = \xi\xi_i, \qquad \bar{\eta} = \eta\eta_i, \qquad \bar{\zeta} = \zeta\zeta_i,$$

and ξ_i, η_i, and ζ_i are the normalized coordinates of the ith node.

The underlying idea of enriching a lower-order element lies in attempting to yield a more stiff system. The remaining question is to check whether this element has the inf-sup condition. In view of the difficulty of analytic verification, we are led to perform numerical experiments to study whether the inf-sup condition is accommodated to this element.

3.1.1.2. Trilinear-pressure/tri-quadratic Lagrangian element (or 27/8 element). Following the same line, we can continue adding velocity nodal points, on each of the 12 edges, to the above-mentioned 15/8 element. This leads to 27 velocity nodal points. This element can be thought of as a tri-

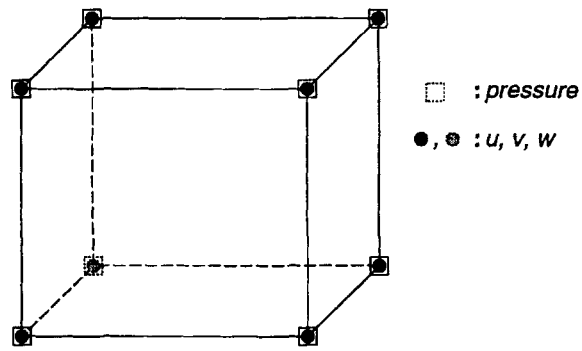

Figure 6. Primitive variables stored in a 8/8 element

quadratic Lagrangian element. The following N^i, which are nodal basis functions, have the property that $N^i(x_j) = \delta^i_j$:

$$N_i = (\tfrac{3}{2}\bar{\xi}^2 + \tfrac{1}{2}\bar{\xi} + 1 + \xi^2 - \xi_i^2)(\tfrac{3}{2}\bar{\eta}^2 + \tfrac{1}{2}\bar{\eta} + 1 + \eta^2 - \eta_i^2)(\tfrac{3}{2}\bar{\zeta}^2 + \tfrac{1}{2}\bar{\zeta} + 1 + \zeta^2 - \zeta_i^2). \tag{15}$$

The major complication with this element is the dramatic increase of matrix size and the prohibitive computational cost. Regardless of this drawback, we still prefer to advocate this element. The main reason is attributable to the accessible error consistency since velocity derivatives are one order higher than those of the pressure.

3.1.2. Discontinuous pressure elements. When a lower-order pressure element is advocated, it is natural to replace eight pressure corner nodes solely with one located at the centroid of hexahedral element. This leads to a piecewise constant pressure element. Under these circumstances, we can dispense with some velocity degrees of freedom; otherwise, the element of interest becomes less constrained. Certainly, the task of judiciously eliminating these dispensable velocity degrees of freedom should be explored and is the focus of our attention. Successful elimination of these dispensable velocity degrees of freedom depends on the presence of the Babuška-Brezzi condition. In addition, the computational efficiency should be simultaneously taken into account. From the view point of programming complexity, we can then build the degenerated variants of the two elements presented in section 3.1.1.

3.1.2.1. $Q_1^+P_0$ element (or 14/1 element). On examining the three momentum equations, one can firstly dispense with the three velocity components at the centroid node of element 15/8, on which we only place the pressure degree of freedom. In the momentum equations, each pressure gradient $\partial p/\partial x_i$ has an influence on the flow motion along the x_i direction respectively. Consequently, the two velocity components on each face of element 15/8 have little or no effect on the flow motion because they have nothing to do with the pressure difference along the direction normal to that surface. Because of these restricted facial degrees of freedom, the resulting element belongs to the so-called multivariant finite element.[19] In this class of elements, some velocity nodes may involve different degrees of freedom. In this discontinuous pressure element, there exists only one degree of freedom on each mid-face node whereas three degrees of freedom are lodged on each vertex of the hexahedron. For this element, the reader is referred to Gupta *et al.*[19] for additional details. For purposes of comparison, we only restrict finite-element meshes to cubical finite elements. This class of elements is characterized as having finite element edges which are parallel to the Cartesian coordinates. In this regard, the shape function can be written by the following form:

Corner node:

$$N_i = \tfrac{1}{8}(1 + \bar{\xi})(1 + \bar{\eta})(1 + \bar{\zeta})[2(\bar{\xi} + \bar{\eta} + \bar{\zeta} - 1) - \bar{\xi}\bar{\eta} - \bar{\eta}\bar{\zeta} - \bar{\zeta}\bar{\xi}]. \tag{16a}$$

Mid-face node:

$$N_i = \tfrac{1}{2}(1 + \bar{\xi} + \bar{\eta} + \bar{\zeta})(1 - \xi^2 + \bar{\xi}^2)(1 - \eta^2 + \bar{\eta}^2)(1 - \zeta^2 + \bar{\zeta}^2). \tag{16b}$$

3.1.2.3. $R_2^+P_0$ element (or 26/1 element). In the same spirit, one can also discard some velocity degrees of freedom to build an element which still satisfies the Babuška–Brezzi condition. The R^+P_0 element given by Gupta *et al.*[19] can be regarded as the degenerated version of element 27/8. This element is attainable by deactivating three velocity components at the centroid node, two velocity components at each mid-face node, and one velocity component parallel to the mid-edge from element 27/8. Owing to the restricted velocity degrees of freedom, this element is still classified as multivariant in nature. In this multi-variant element, the derived basis functions turn out to be those in Reference 19. Also of note is that, we only apply this element to cubical finite-element meshes as the element discussed in 14/1.

Table I. Constraint ratio

element type	27/8			26/1			14/1		
number of element	4^3	8^3	16^3	4^3	8^3	16^3	4^3	8^3	16^3
number of point	9^3	17^3	33^3	9^3	17^3	33^3	9^3	17^3	33^3
number of total variables	2312	15468	112724	1279	8315	59635	679	4427	31891
number of computed velocities	1029	10125	89373	441	4725	43245	225	2373	21645
number of computed pressures	124	728	4912	63	511	4095	63	511	4095
number of boundary conditions	1159	4615	18439	775	3079	12295	391	1543	6151
constraint ratio	8·2984	13·9080	18·1948	7·0000	9·2466	10·5604	3·5714	4·6438	5·2857

Corner node:

$$N_i = \tfrac{1}{8}(1+\bar{\xi})(1+\bar{\eta})(1+\bar{\zeta})(\bar{\xi}\bar{\eta}+\bar{\eta}\bar{\zeta}+\bar{\zeta}\bar{\xi}+1-\bar{\xi}-\bar{\eta}-\bar{\zeta}). \tag{17a}$$

Mid-edge node:

$$N_i = \tfrac{1}{4}(1+\bar{\xi})(1+\bar{\eta})(1+\bar{\zeta})(\bar{\xi}+\bar{\eta}+\bar{\zeta}-1)(1-\xi^2+\bar{\xi}^2)(1-\eta^2+\bar{\eta}^2)(1-\zeta^2+\bar{\zeta}^2). \tag{17b}$$

Mid-face node:

$$n_I = \tfrac{1}{2}(1+\bar{\xi}+\bar{\eta}+\bar{\zeta})(1-\xi^2+\bar{\xi}^2)(1-\eta^2+\bar{\eta}^2)(1-\zeta^2+\bar{\zeta}^2). \tag{17c}$$

3.2. Constraint counts on the investigated elements

As discussed earlier, an accommodation of interpolations for velocity and pressure in the incompressible equations may be inappropriate. *A priori* knowledge of a good match between these primitive variables is, thus, requisite. While the adoption of the LBB stability condition can provide us with information to affirm whether or not an element will lock, to establish such verification is not a trivial task and is often beyond the ability of many finite element practioners. For this reason, the method of constraint count, which has been proven quite effective in providing us with a hint regarding the onset of erroneous pressure, will be adopted to roughly determine the applicability of the employed element.

As is usual, we shall employ the constraint ratio, defined by

$$\lambda = n_v/n_{in}, \tag{18}$$

to estimate the propensity for locking. In equation (18), n_v represents the total number of velocity equations after the boundary velocities are specified while n_{in} represents the total number of incompressibility constraints. In three dimensions, an element of constraint ratio λ smaller than 3 will tend to lock. As λ continues to decrease to $\lambda \leqslant 1$, the lock phenomenon will be anticipated.

The value of λ for a given set of interpolation functions varies with the number of elements per side. The larger the problem size is, the larger the value of λ is. This implies that the tendency for locking is associated with the problem size. With this fact in mind, we have summarized the computed λ, together with the degrees of freedom of primitive variables, in Table I for the investigated elements, $4 \times 4 \times 4$, $8 \times 8 \times 8$, and $16 \times 16 \times 16$.

At this point, it is important to note that the above approach in assessing the ability of an element is not a precise mathematical means. In practical computations, different conclusions regarding convergent behaviour might arise judging from different methods of constraint count. In order to make a clear comparison, we have carried out a series of calculations, which will be described in the result section, for checking if the convergent solution is attainable. It is appropriate at this point to derive the analytic constraint ratio for each element under consideration. Apart from the three elements discussed earlier, we also consider 8/1, 8/8, and 15/8 elements for purpose of comparison. In Table II, we have

Table II. Constraint ratio

element type		$\lambda(n)$	patch test range of $\lambda(n) > 1$		analytic test
uni-variant	8/1	$\frac{3n^3 - 9n^2 + 9n - 3}{n^3 - 1}$	$1 < \lambda < 3^*$	$4 \leqslant n$	—
	8/8	$\frac{3n^3 - 9n^2 + 9n - 3}{n^3 + 3n^2 + 3n}$	$1 < \lambda < 3^*$	$6 \leqslant n$	—
	15/8	$\frac{15n^3 - 18n^2 + 9n - 3}{n^3 + 3n^2 + 3n}$	$1 < \lambda < 15^*$	$2 \leqslant n$	failure
	27/8	$\frac{24n^3 - 36n^2 + 18n - 3}{n^3 + 3n^2 + 3n}$	$1 < \lambda < 24^*$	$2 \leqslant n$	success
multi-variant	14/1	$\frac{6n^3 - 12n^2 + 9n - 3}{n^3 - 1}$	$1 < \lambda < 6^*$	$2 \leqslant n$	success
	26/1	$\frac{12n^3 - 24n^2 + 15n - 3}{n^3 - 1}$	$1 < \lambda < 12^*$	$2 \leqslant n$	success

* indicates the upper bound for the value of constraint ratio as n approaches infinity

tabulated the analytic constraint ratios which are functions of the number of elements along one side. In a pack of elements, the minimal value of n for which an investigated element can pass the patch test is also included in Table II. We have also calculated the values of λ in terms of the number of elements per side. The lower bound for an element passing the patch test is 1.

By examining the estimated constraint ratios, as shown in Figure 7, we find that the value of $\lambda \mid_{14/1}$ is always smaller than that of $\lambda \mid_{26/1}$ as far as multi-variant elements are concerned. This implies that element 14/1 has a higher percentage of incompressibility constraints. For the investigated uni-variant elements, the constraint ratio of element 15/8 is smaller than that of element 27/8. The constraint ratios of univariant elements are larger than the values of multivariant elements when n becomes larger than 9, as shown in Figures 7 and 8. For the same number of pressure unknowns, the value of $\lambda \mid_{27/8}$ is greater than that of $\lambda \mid_{26/1}$ when n is larger than 3, and the value of $\lambda \mid_{15/8}$ is greater than $\lambda \mid_{14/1}$ as n turns out to be larger than 2. It is of note that elements 27/8 and 15/8 have the same number of pressure unknowns, $(n+1)^3 - 1$, for n elements in one coordinate. Also of note is that elements 26/1 and 14/1 have the same pressure unknowns, $n^3 - 1$, for a fixed n.

3.3. Test functions in SUPG finite element model

Numerical errors common to flow simulations of high Peclet number can be well-suppressed with the use of upstream weighted test functions. By appealing to the physical analogy, we find that more artificial diffusion must be added along the flow direction to enhance the stability because the stiffness matrix becomes more diagonally dominant. This is not a problem in one-dimensional flow simulation. In multidimensional cases, the situation is much more complicated because neither the upwinding direction nor its associated upwinding coefficient is easy to attain. An analytical derivation of τ for a truly multi-dimensional analysis is still being studied. In the present study, the expression of τ is derived based on the assumption of operator splitting. The following amount of τ is spanned by an analytic representation along each direction[21]

$$\tau = \tilde{\alpha}/|V|^2, \tag{19}$$

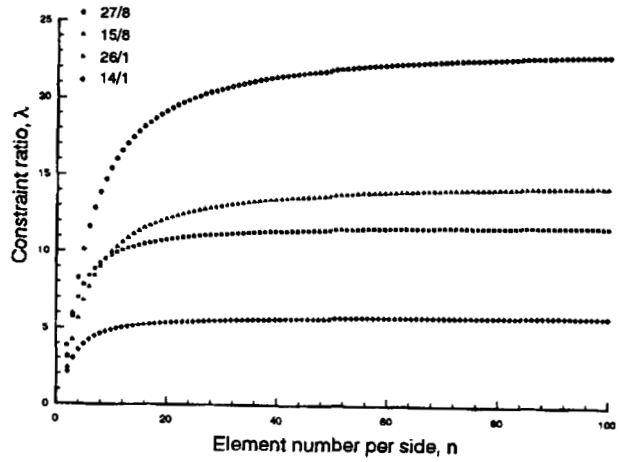

Figure 7. Constraint ratio for 27/8, 15/8, 26/1, and 14/1 elements against the number of element per side, n.

where

$$\bar{\alpha} = (\alpha_\xi V_\xi h_\xi + \alpha_\eta V_\eta h_\eta + \alpha_\zeta V_\zeta h_\zeta)/2, \quad |V|^2 = V_j V_j,$$

$$\alpha_\xi = f(\gamma_\xi), \alpha_\eta = f(\lambda_\eta), \alpha_\zeta = f(\gamma_\zeta),$$

$$\gamma_\xi = V_\xi h_\xi Re/2, \gamma_\eta = V_\eta h_\eta Re/2, \gamma_\zeta = V_\zeta h_\zeta Re/2,$$

$$V_\xi = \hat{\mathbf{e}}_\xi \cdot V, V_\eta = \hat{\mathbf{e}}_\eta \cdot V, V_\zeta = \hat{\mathbf{e}}_\zeta \cdot V,$$

$$f(\gamma) = \tfrac{1}{2}\coth(\tfrac{1}{2}\gamma) - \frac{1}{\gamma}. \tag{20}$$

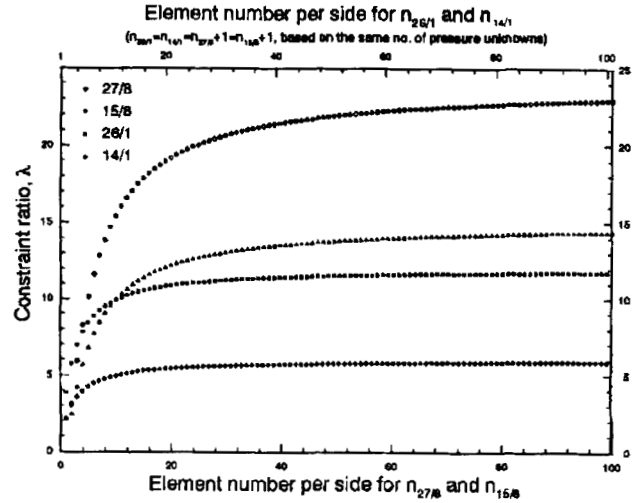

Figure 8. Constraint ratio for 27/8, 15/8, 26/1, and 14/1 elements against the number of element per side, n, based on the same number of pressure unknowns

3.4. *Solution solver*

The main deficiencies, as compared with the segregated solution algorithm, encountered in the mixed formulation comprise a high disk-storage requirement and large CPU time per iteration. In consequence, a direct solver of the frontal type may not be advantageous in solving a large-size problem where matrix equations of non-symmetric and indefinite form are encountered. Most classical iterative solvers are generally not amenable to convergent solution. It seems logical to turn to modern iterative solvers such as the bi-conjugate gradient stable iterative method (Bi-CGSTAB[22]). However, iterative solvers pose the considerable difficulty of removing the near breakdown, which is a currently active research topic. For this reason, we use only the direct solution solver in what follows for small-size problems ($4 \times 4 \times 4$ and $8 \times 8 \times 8$) and the Bi-CGSTAB[22] iterative solver for large-size problems.

4. COMPUTED RESULTS

To carry out a performance study, it is necessary to choose a model problem, implemented on different types of elements. Attention will first be given to validating the computer code by solving a problem amenable to close-form solution. Secondly, the order of solution accuracy and the rate of solution accuracy will then be computed accordingly. For the entire surface of a square cubical cavity of length 1, we specify the discrete values of velocity according to the following expressions:

$$u = \tfrac{1}{2}(y^2 + z^2), \quad v = -z, \quad w = y. \tag{21}$$

With these boundary conditions of the Dirichlet type, the pressure takes the following form:

$$p = \tfrac{1}{2}(y^2 + z^2) + \frac{2}{Re}x. \tag{22}$$

The disparity between the computed and analytic solutions has been measured in terms of L_2-norm. Three uniform grids were investigated to estimate the rates of convergence. As seen from the computed error norms and convergent orders, given in Tables III and IV, there is good agreement with the analytic solution. Of note is that the solutions for the investigated element, $16 \times 16 \times 16$, were obtained from the Bi-CGSTAB iterative solver under the convergent tolerance of 10^{-10} and the tolerance of nonlinear outer iteration 10^{-6}. The amount of time used on the CRAY X-MP EA/116se is presented in Table IV to assess the effectiveness of the investigated elements.

Before discussing solutions computed from a 27/8 uni-variant element, and multi-variant elements 26/1 and 14/1, it is worthwhile to explain why we fail to obtain a convergence solution from the investigated 15/8 uni-variant element. It should be emphasized that an element passing the constraint test may fail to yield a convergent solution. One can extract the inner brick from a pack of eight basic

Table III. Error of L_2 norm

element type		number of element 4^3	8^3	16^3
27/8	$\underline{u}$	$8{\cdot}46708 \times 10^{-3}$	$4{\cdot}69061 \times 10^{-3}$	$2{\cdot}27517 \times 10^{-3}$
	p	$2{\cdot}99745 \times 10^{-2}$	$1{\cdot}40210 \times 10^{-2}$	$7{\cdot}15795 \times 10^{-3}$
26/1	$\underline{u}$	$9{\cdot}91253 \times 10^{-3}$	$4{\cdot}99803 \times 10^{-3}$	$2{\cdot}33302 \times 10^{-3}$
	p	$3{\cdot}15788 \times 10^{-2}$	$1{\cdot}44566 \times 10^{-2}$	$6{\cdot}53394 \times 10^{-3}$
			$5{\cdot}49845 \times 10^{-3}$	$2{\cdot}46413 \times 10^{-3}$
14/1	$\underline{u}$	$1{\cdot}15789 \times 10^{-2}$	$1{\cdot}43048 \times 10^{-2}$	$6{\cdot}32338 \times 10^{-3}$
	$\underline{p}$	$3{\cdot}06003 \times 10^{-2}$		

Table IV. Convergent order and CPU time

element type			number of element 4^3	8^3	16^3
27/8	*co**	$\underline{u}$		0·8521	1·0438
		p		1·0961	0·9700
	CPU		1044	16929	180935†
26/1	*co*	$\underline{u}$		0·9879	1·0992
		p		1·1272	1·1457
	CPU		294	7313	454963†‡
14/1	*co*	$\underline{u}$		1·0744	1·1579
		p		1·0970	1·1777
	CPU		186	3245	32743

* *co* denotes the convergent order
† the solution is solved by BiCGStab iterative method
‡ the solution is obtained under the outer iterative convergent tolerance of 10^{-4}

15/8 elements, as shown in Figure 9. On each surface of the extracted brick, there are no velocity nodal points to store velocities as the result of pressure gradient setup from the adjacent center pressure nodes. It suffices to say that with the mid-face velocity nodal points, which are useful in stabilizing the incompressible system, oscillatory solutions are still expected owing to the lack of mid-surface velocity nodes as shown in Figure 9(b).

The cost-effectiveness of the solution is, to a large extent, dependent on the programming complexity. While generating a data structure for multi-variant elements of even simple form can be a tedious and time-consuming task, we still prefer this class of elements mainly because of the computing time, as seen in Table 4, which is saved if a direct solver is considered. The computer resources in CPU, I/O, memory and disk storage become prohibitively large (about 50,000 unknowns)

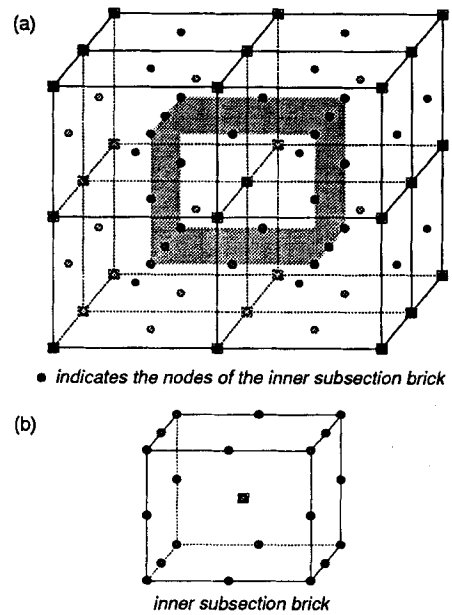

Figure 9. (a) A brick containing eight 15/8 elements; (b) inner extracted brick

when mesh numbers are increased to $16 \times 16 \times 16$, and the use of a frontal solver is no longer advantageous.

For a problem with a fixed number of elements, element 27/8 is most storage intensive, followed by element 26/1 and element 14/1 respectively. The amount of computing time involved in the solution of linear equations, either using a direct or an iterative method, follows the same trend as that of the storage requirement. As seen from the computed L_2 error norms, little variation exists between the investigated elements under the condition that the element number per side is fixed.

Through these computations, we fail to obtain convergent solution from elements 15/8. This means that the success of a patch test does not necessarily assure convergence solutions. The failure to obtain convergent solutions in elements 8/1 and 8/8 can be attributed to the lack of velocity nodes on the centroid of the control surface. This shows that this type of mesh arrangement can not respond to the existing pressure gradient.

5. CONCLUSIONS

In this paper we have been concerned with the incompressible Navier–Stokes equations in three dimensions. Attention has been directed to assessing the smoothness of pressure and the rate of convergence for every investigated element. Two classes of velocity/pressure elements have been studied, namely the tri-linear continuous pressure element and the multivariant element, which belong to the discontinuous pressure element. In each class, two variants were considered. For the multi-variant elements Q^+P_0 and $R^0_+P_0$, they are the simplified forms of elements 15/8 and 27/8 respectively. From the equations considered and the test problem analysed, we can draw the following conclusions.

1. Even though the programming effort is laborious, we prefer using the multi-variant element because of the computing time it can save when using a frontal direct solver. As for a larger size problem, the above statement might not be true. It heavily depends on the iterative solver used and the stiffness matrix rendered.

2. The rationale behind the use of the multi-variant element is two-fold. First, we assign indispensable velocity nodal points for a fixed pressure node. Second, it is not necessarily to provide more than the sufficient velocity degrees of freedom. It follows that one can obtain quite smooth convergent pressure from smaller size matrix equations. Of course, one can obtain solutions of higher resolution from uni-variant elements, at the cost of the demand for a larger storage capacity to solve the matrix equations. If the direct solver is considered only, there exists a trade off between less programming complexity using uni-variant elements and less laborative computing effort when dealing with multi-variant elements.

3. Even though they pass the patch test, elements 8/1, 8/8, and 15/8 still fail to render convergence solutions. This implies that the realm of patch-test-satisfaction is much larger. An element with the *LBB* stability condition can pass the patch test. The opposite is not necessarily true. Also of note is that, if an element fails to pass the patch test, then it should be classified as a singular stiffness matrix.

REFERENCES

1. M. D. Gunzburger, *Finite Element Methods for Viscous Incompressible Flows, A Guide to Theory, Practice, and Algorithms*, Academic Press, Inc., 1989.
2. G. F. Carey and J. T. Oden, *Finite Elements: Fluid Dynamics*, vol. VI, Prentice-Hall, Englewood Cliffs, NJ, 1986.
3. O. Pironneau, *Finite Element Methods for Fluids*, John Wiley and Sons, Chichester, 1989.
4. T. J. R. Hughes, W. K. Liu, and A. Brooks, 'Finite element analysis of incompressible viscous fluid by the penalty function formulation,' *J. Comp. Phys.*, **30**, 1–60 (1979).
5. B. N. Jiang and L. A. Povinelli, 'Least-squares finite element method for fluid dynamics', *Comput. Methods Appl. Mech. Eng.*, **81**, 13–37 (1990).

6. B. N. Jiang, 'A Least-squares finite element method for incompressible Navier-Stokes problems', *Int. j. numer. methods fluids*, **14**, 843–859 (1992).
7. R. Teman, *Navier-Stokes Equations, Theory and Numerical Analysis*, North-Holland, Amsterdam, Rev. edition, 1979.
8. V. Girault and P. A. Raviart, *Finite Element Methods for Navier-Stokes Equations*, Springer–Verlag, Berlin, 1986.
9. A. J. Chorin, 'A numerical method for solving incompressible viscous flow problems', *J. Comp. Phys.*, **2**,12–26 (1967).
10. P. M. Gresho and R. L. Sani, 'On pressure boundary conditions for the incompressible Navier-Stokes equations', *Finite Elements in Fluids*, **7**, 123–157 (1987).
11. P. M. Gresho, 'Some current CFD issues relevant to the incompressible Navier-Stokes equations', *Comput. Methods Appl. Mech. Eng.*, **87**, 201–252 (1991).
12. R. L. Sani, P. M. Gresho, R. L. Lee, D. F. Griffiths, and M. Engleman, 'The cause and cure (?) of the spurious pressures generated by certain FEM solutions of the Navier-Stokes equations, Parts II', *Int. j. numer. methods fluids*, **1**, 171–204 (1981).
13. F. Brezzi, 'On the existence, uniqueness and approximation of saddle point problems arising from Lagrangian multipliers', *RAIRO, Anal. Num.*, **8**, (R2), 129–151 (1974).
14. Babuška, 'Error bounds for finite element methods', *Numer. Math.*, **16**, 322–333 (1971).
15. T. J. R. Hughes, L. P. Franca, and M. Becestra, 'A new finite element formulation for computational fluid dynamics, V. circumventing the Babuška–Brezzi condition, A stable Petrov-Galerkin formulation of the Stokes problem accommodating equal-order interpolations', *Comput. Methods Appl. Mech. Eng.*, **59**, 85–99 (1986).
16. D. A. Anderson, J. C. Tannehill, and R. H. Pletcher, *Computational Fluid Mechanics and Heat Transfer*, Hemishere Publishing Co., 1984.
17. T. B. Gatshi, C. E. Grosch, and M. E. Rose, 'A numerical study of the two-dimensional Navier-Stokes equations in vorticity-velocity variables', *J. Comp. Phys.*, **48**, 1–22 (1982).
18. K. Aziy and J. D. Hellums, 'Numerical solution of the three-dimensional equations of motion for laminar natural convection', *Phys. Fluids*, **10**, 314–324 (1967).
19. M. Gupta, T. H. Kwon, and Y. Jaluria, 'Multivariant finite elements for three-dimensional simulation of viscous incompressible flows', *Int. j. numer. methods fluids*, **14**, 557–585 (1992).
20. D. Pelletier, A. Garon, A. Fortin, F. Bertrand, and P. Tanguy, 'Numerical Methods in Laminar and Turbulent Flow', *Proceedings of the Sixth International Conference*, **6**, 1803–1813, Swansea (1989).
21. T. W. H. Sheu and M. M. T. Wang, 'A Validation Study of Quadratic SUPG Formulation for Incompressible Viscous Flows', K. Morgan *et al.*, editor, *VIII International Conference on Finite Elements in Fluids*, 224–232, Barcelona, Sep. (1993).
22. H. A. Van der Vorst, 'BI-CGSTAB: A fast and smoothly converging variant of BI-CG for the solution of nonsymmetric linear systems', *SIAM J. Sci. Statist. Comput.*, **13**, 631–644 (1992).